Experimental evidence concerning the significant information depth of X-ray diffraction (XRD) in the Bragg-Brentano configuration

Wolfgang Wisniewski, Cécile Genevois, Emmanuel Veron, Mathieu Allix

Experimental evidence concerning the significant information depth of X-ray diffraction (XRD) in the Bragg-Brentano configuration

Wolfgang Wisniewski [1,2,a] Cécile Genevois,[1] Emmanuel Veron,[1] and Mathieu Allix[1]
[1]CNRS, CEMHTI UPR3079, University Orléans, F-45071 Orléans, France
[2]Le Studium Research Fellow, Loire Valley Institute for Advanced Studies, Orléans & Tours, France

(Received 7 June 2022; accepted 10 January 2023)

X-ray diffraction in the Bragg-Brentano configuration ("XRD") is a very established method. However, experimental evidence concerning its significant information depth, i.e. microstructure components from which maximum depth can affect the information evaluated from the acquired diffraction pattern, are scarce in the scientific literature. This depth is relevant to all XRD measurements performed on compact samples, especially layered composites and samples showing a crystallographic texture evolution. This article provides experimentally determined upper and lower limits to the significant information depth: XRD patterns acquired from a compact crystal layer through a layer of compact, amorphous glass indicate that the significant information depth of XRD using Cu $K_{\alpha 1}$ and $K_{\alpha 2}$ radiation is very likely larger than 48 µm, but smaller than 118 µm, in a material of the composition $Mg_2Al_4Si_5O_{18}$ with a density of ca. ~2.6 g/cm^3. The depth of 48 µm correlates to the depth larger than the layer of material from which 90% of the reflected X-rays originate at $2\Theta = 25.8°$.

[doi:10.1017/S0885715623000052]

Key words: XRD, information depth, Bragg-Brentano setup, cut-off value

I. INTRODUCTION

X-ray diffraction in the Bragg-Brentano configuration (XRD – reflection mode) is a very established method for identifying crystalline phases and is also used to determine the crystal structure and mean crystal size of nm-scale crystals via Rietveld refinements (Holder and Schaak, 2019). It can also be used to detect selected crystallographic textures in unpowdered compact samples and estimate the degree of crystallinity. However, results have shown that XRD may miss certain phase/texture information *(information meaning "facts obtained from investigation") or imply more texture than actually occurs. Examples obtained during the analysis of partially crystallized glasses will be presented below. Principal limits of XRD for texture analysis have been discussed in detail in Chapter 5.1.1 of Wisniewski et al. (2018a).

For example, the topmost, ca. 7 µm thick layer of 101-oriented crystals in surface crystallized Ba-fresnoite was not detected by the widely available "laboratory XRD" in the Bragg-Brentano configuration because the 001-oriented layer beneath it dominates the XRD pattern (Wisniewski et al., 2010a). In the cases of surface crystallized $BaAl_2B_2O_7$ (Wisniewski et al., 2010b) or cristobalite (Wisniewski et al., 2013), crystals grown from the respective glasses show a texture in the topmost layer, initially interpreted to apply to the entire layer of surface crystallization, but later proven to be limited to the immediate surface (Wisniewski et al., 2010b, 2013). Slow texture changes such as those observed during the surface crystallization of Sr-fresnoite (Wisniewski et al., 2012a, 2012b) or $Sr_{0.75}Al_{1.5}Si_{0.5}O_4$ (Wisniewski et al., 2018b) may go undetected unless they are specifically sought after. Additionally, relatively thin crystal layers may go undetected by such XRD analyses if there is a strong signal from a phase at the surface and the bulk is composed of a third phase. Another XRD pattern acquired from the unpowdered surface of a crystallized glass (Keshavarzi et al., 2013) only indicated yttrium aluminum garnet (YAG,$Y_3Al_5O_{12}$ with a layer thickness of max. 60 µm) and some additional weak peaks. Removing the YAG layer and powdering the sample indicated a pattern that may be attributed to the JCPDS file 39-0223 and matches the crystallographic data of α-$Y_2Si_2O_7$ (Hartenbach et al., 2006), i.e. XRD indicated two crystalline phases in this material. In fact, five crystal phases were identified in this material, four of them close to the surface and one not detected by XRD altogether even after it was isolated from the others by grinding (Keshavarzi et al., 2013).

The problems outlined above may be traced to the "significant information depth" of the applied XRD in the Bragg-Brentano configuration. This term is specifically used to emphasize that the signal evaluation contributes to the generated information in contrast to "significant probing depth" or "effective penetration depth" (Liu et al., 2010) which could be understood to only refer to the physical signal generation. It should be remembered that the "significance" is defined either

[a]Author to whom correspondence should be addressed. Electronic mail: wolfgang.w@uni-jena.de

by the applied software and/or the user: some limit must define whether a weak peak is considered part of the noise, or treated as a signal. "The significant information depth" is also an answer to the question: at which distance from the analyzed surface does a signal stop playing a relevant role during the evaluation of an obtained XRD pattern? While the absorption of the X-ray intensity at a given *penetration* depth may be calculated (Henke et al., 1982), this does not really help the practitioner because there is no information about where to define a cut-off value for this function. Obviously, a sudden texture in the deepest 0.1% of the information depth cannot be significant to the XRD pattern evaluation. Despite searching on and off for more than 10 years, the authors mostly found literature, e.g. stating how the absorption may be calculated (Henke et al., 1982; Allmann, 2003; Birkholz, 2006; Spieß et al., 2009) and at best presenting tables illustrating the depths for a selection of materials assuming a residual intensity of 10% (Allmann, 2003) or an absorption of 90% (Spieß et al., 2009), which is basically the same thing. Experimental data on the significant information depth or a reason why e.g. this cut-off value of 10% was chosen is lacking. Alternatively, "penetration depths" of 0.1–10 µm have been stated without any comment on the parameters used in the calculations (Birkholz, 2006) and without noting that the significant information depth must be smaller than the penetration depth for the reason stated above. The outlined issue was, however, addressed by Liu et al. in 2010 but the experiments were limited to incidence angles of 3–5° according to the experimental section. The experiments were performed using layers of compacted crystalline organic materials and thus making the following assumptions: densification was homogeneous throughout the sample and did not introduce a texture, X-ray interaction with gasses in pores can be neglected and the layer thicknesses calculated from the sample geometry and mass are correct. The applied materials are suitable for the analysis as their characteristic peaks do not overlap in XRD patterns.

A study concerning the surface crystallization of pure SiO_2 glass using Cu Kα radiation and $10° \leq 2\Theta \leq 60°$ implied that a cut-off value of 40% might result in more realistic calculations (Wisniewski et al., 2013). There is quite a difference between these values: for SiO_2, a cut-off value of 10% results in a depth of more than 250 µm while a 40% cut-off value leads to a depth of about 100 µm. At the same time, Renoirt et al. (2019) state that "the significant information depth of the X-rays . . . is about 10 µm" based on calculations concerning glass-ceramics containing Sr-fresnoite without stating any parameters of the latter. Liu et al. (2010) stated that the signal from a layer of α-lactose monohydrate could be detected through a 176 µm thick layer of mannitol while a 239 µm thick layer of mannitol blocked any signal from the crystalline material below it, the densities are $\approx$1.5 g/cm^3 (Liu et al., 2010). Of course, the absolute difference between the various cut-off values should become less important with a smaller information depth, e.g. with growing material densities and X-ray absorption coefficients. It is, however, clear that there are cases where the significant information depth is relevant to the ability to detect textures or phases occurring at different depths in compact samples.

The information depth of XRD depends on the incident angle of the radiation because the constant path length for a given degree of absorption reaches increasing depths for entry angles from 0% of the maximum information depth at 0° (parallel beam not entering the material) to 100% at 90°. The size of the information volume, however, is kept as constant as possible during the measurements by applying a slit with a constant aperture to the X-ray beam: at low angles, the interaction area is large while the depth is small, and at large angles, the area is small but the depth is large. For the generally analyzed powders, the amount of analyzed material thus remains relatively constant. In compact samples containing multiple layers, the increasing information depth can lead to the inclusion of different phases or texture components during a measurement.

The XRD practitioner is primarily interested in the "*maximum* significant information depth" so as to be on the safe side of what may affect a performed measurement. The maximum penetration depth is reached at an incident angle of 90°. The significant information depth, however, only considers the signal intensity of the reflected X-rays and the 2Θ-values of the compound-specific diffraction peaks whose intensities dramatically decrease as 2Θ approaches 90° in this setup. Including all possible aspects into this complex consideration quickly goes beyond a practical way of estimating the correct *maximum* significant information depth.

Hence, the aim of this article is to (a) present an experimental setup useful for acquiring information about the significant information depth of XRD and (b) deduce cut-off values defining minimum and maximum boundaries for calculations of the penetration depth that correlate to these experimental results so that they may be transferred to other materials and radiations.

Surface crystallizing glass ceramics such as cordierite (Wisniewski et al., 2011) provide suitable materials to answer this question, as it is possible to produce a crystal layer of a reasonably well-defined thickness in direct contact to an amorphous glass of a very similar mean atomic density and hence X-ray absorbance. If XRD is performed from the glass side of such a sample, an X-ray amorphous layer covers a crystalline layer and the thicknesses of both layers are easy to determine. If the thickness of the glass layer is continuously decreased, XRD peaks must become detectable at some point. As long as no XRD peaks are detected, the significant information depth of XRD is smaller than the thickness of the glass layer. When the first XRD peak is detected, the significant information depth of the performed XRD measurement must be larger than the thickness of the covering glass layer as the X-rays must penetrate it, be diffracted by the crystal layer and re-penetrate the amorphous layer to reach the detector and produce a signal.

Assuming the difference for X-ray scattering between the glass and µ-cordierite is negligible, the cut-off value leading to the same depth in calculations of the penetration depth should be transferrable to calculations for other phases as they are based on the Lambert-Beer Law. Assuming the influence of the applied equipment can be neglected, this simplified approach avoids the complications of calculating degrees of absorption for the incoming and reflected radiation, peak intensity competition from another crystal phase, density differences, and so on.

II. EXPERIMENTAL

A sample was cut from a glass block with the stoichiometric composition of cordierite and ground to a thickness

https://doi.org/10.1017/S0885715623000052 Published online by Cambridge University Press

of $3 \times 15 \times 15$ mm^3. One of the large surfaces was then ground with abrasive SiC discs down to a final step with a grain size of 6 µm. The sample was subsequently crystallized at 910 °C for 3 h in an electrical furnace (Nabatherm P320) under a normal laboratory atmosphere (air) to grow the desired layer of crystallization (Wisniewski et al., 2011). All crystal layers except the one grown on the previously polished surface were subsequently removed by grinding.

After acquiring a reference XRD pattern from the remaining crystal layer, the crystalline surface of the sample was fixed on a plane-parallel sheet of glass and this stack was embedded using Araldite 2020. Then, the stack was ground from the glass side of the sample to obtain two plane-parallel surfaces. As this stack would become very thin during the intended experiment, and hence difficult to handle, a supporting layer of Araldite 2020 was added under the supporting glass sheet, again maintaining the plane-parallel shape. Subsequently, material was removed from the glass side of the sample until only ca. 1 mm of glass remained above the crystal layer.

The resulting sample, prepared according to the setup illustrated in Figure 1, was positioned on the XRD sample holder and an initial XRD pattern was acquired. Subsequently, the thickness of the glass layer covering the crystal layer was successively decreased between measurements until an XRD pattern containing the peaks indicating crystallization was acquired. The height of the sample surface was held constant with respect to the Bragg-Brentano focusing circle as well as possible using a homemade screw-based positioning system.

The XRD patterns were acquired using a Bragg-Brentano D8 Advance Bruker diffractometer which has a 237.5 mm radius using a Cu anode ($K_{\alpha 1}$ (8047.8162(4) eV) and $K_{\alpha 2}$ (8027.9435(2) eV) radiation (Mendenhall et al., 2017)) equipped with a LynxEye XE detector over an angular range of $10° \leq 2\theta \leq 60°$. The anode voltage and current were fixed at 40 kV and 40 mA (1.6 kW). The divergence slit was chosen to be open by 0.5° so that the beam would always be wider than the sample in the analyzed range (max. beam width = 11.94 mm). The final XRD patterns were collected using a step size of 0.016° with an acquisition time of either 1.1 s per step (total measurement time of ~1 h) or of 13.3 s per step (total measurement time of ~12 h).

After the µ-cordierite layer was detected by XRD, cross sections of the sample were polished, coated with a thin layer of carbon and analyzed using a Merlin compact Zeiss Gemini Scanning Electron Microscope (SEM). The cross sections were analyzed using a backscattered-electron (BSE) detector at a working distance of 10 mm in order to measure the thickness of the sample as well as the thickness of the crystallized layer. A µm screw (Whitworth, ±10 µm) was used to measure the lengths of the sample sides which will be stated below. Subsequently, the final XRD patterns were acquired using measurement times of 1 and 12 h.

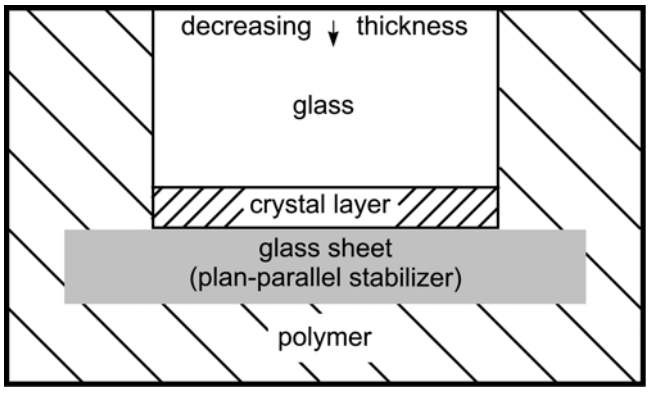

Figure 1. Schematic illustration of the sample setup measured in the diffractometer.

Attenuation calculations were performed using the program AbsorbDX (DIFFRAC.EVA V3.1) using the radiation stated above and the material composition of µ-cordierite ($Mg_2Al_4Si_5O_{18}$) with a density of 2.62 g/cm (Wisniewski et al., 2010a) and a mass attenuation coefficient of 33.28 cm^2/g.

III. RESULTS AND DISCUSSION

The stoichiometric cordierite glass is well suited for the proposed experiments because it is easy to produce well defined, initially untextured layers of µ-cordierite (Wisniewski et al., 2011) which almost have the same density (2.59 g/cm^3) and chemistry (in mol: $2Al_2O_3 \cdot 2MgO \cdot 5SiO_2$) as the uncrystallized glass (2.62 g/cm^3). µ-cordierite crystallizes from the surface of the selected glass without significant surface deformations, cracks or any chance of bulk crystallization. The cordierite system is a model system for crystal nucleation and growth in glasses (Diaz-Mora et al., 2000; Müller et al., 2000; Pannhorst, 2000; Fokin et al., 2006) and has been extensively analyzed with XRD in the Bragg-Brentano setup. Although surface crystallizing glasses frequently show oriented nucleation at the surface (Wisniewski and Rüssel, 2021), µ-cordierite does not show this phenomenon (Wisniewski et al., 2011) but a texture resulting from growth selection has been reported (Diaz-Mora et al., 2000). In order to grow an appropriate layer of µ-cordierite, the glass was crystallized at 910 °C for 3 h (Wisniewski et al., 2011) and treated as outlined in the Experimental section.

Figure 2 presents selected XRD patterns acquired during the performed experiments as well as the theoretical pattern of µ-cordierite for reference. The XRD pattern (a) acquired from the initial, crystallized surface shows the sole presence of µ-cordierite and, in agreement with previous experiments, a texture is not indicated. It shows a shift to lower 2Θ values due to a small mismatch in the sample position, i.e. its height. The XRD patterns acquired when the sample had a total thickness of 1 mm and before the last polishing step, which removed ca. 70 µm of material, are presented to confirm that there was no sign of bulk nucleation, which is in agreement with the literature. The XRD patterns acquired from the final sample for 1 or 12 h both show a strong µ-cordierite pattern, a strong "glass mound" and a peak shift to the right compared with the surface pattern which results from a slightly different height (z-position) of the analyzed sample. One significant difference between them is that measuring for 12 h enhances the signal-to-noise ratio but it is also discernible that the (101) peak shows a stronger relative intensity after 12 h than after 1 h. Such relative peak enhancements indicate crystallographic textures and a 101 texture of cordierite was also reported by Diaz-Mora *et al.* in 2000 after removing ca. 10 µm of crystallization from the surface. Such slight intensity variations can e.g. result from small differences in the sample position. It is also noteworthy that the peak at $2\Theta = 19.76°$ is

https://doi.org/10.1017/S0885715623000052 Published online by Cambridge University Press

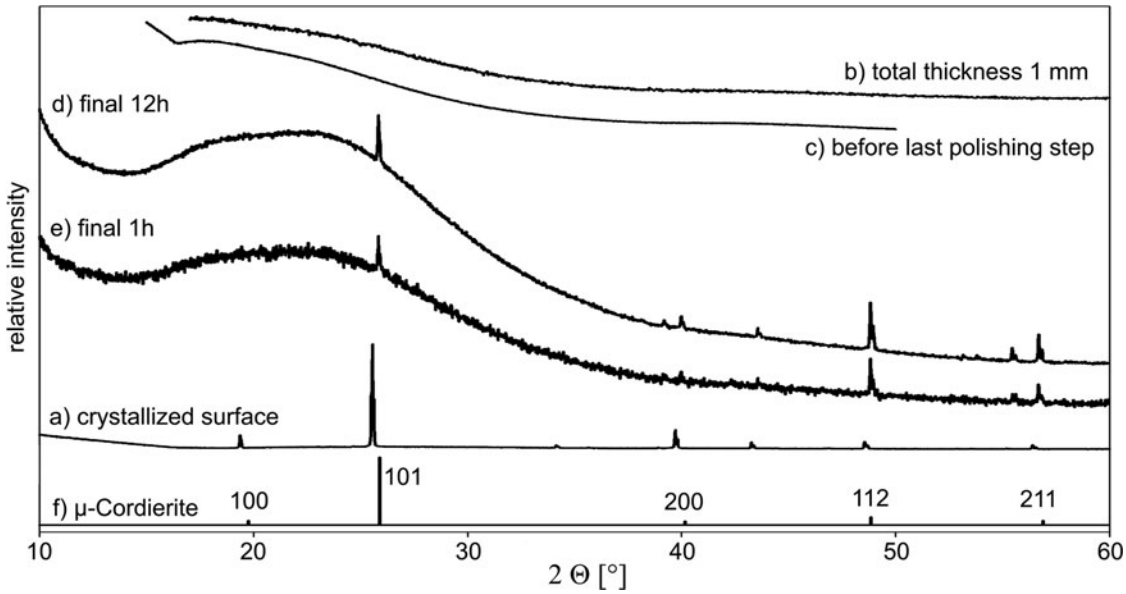

Figure 2. XRD patterns acquired from (a) the crystallized surface of the prepared sample as well as (b) from the glass side of the prepared sample with a total thickness of 1 mm and (c) before the last polishing step. The patterns acquired from the glass side of the sample after the final polishing step are presented after measurements acquired for (d) 12 h or (e) 1 h. The theoretical pattern (f) of μ-cordierite (JCPDS file No. 01-073-2338) is presented for comparison and the lattice planes corresponding to the respective peaks are noted.

not discernible while the peaks at $2\Theta > 45°$ show exaggerated intensities. This can be explained by the angle-dependent information depth of the method: small entry angles lead to a smaller information depth than large entry angles so that the glass layer dampens the signal less as the incidence angle approaches perpendicularity.

Before acquiring of the final XRD patterns (d) and (e), cross sections of the sample were prepared and analyzed by SEM. The SEM micrographs in Figure 3 represent these cross sections: the initially polished surface in contact with the μ-cordierite crystals is at the bottom while the glass layer covering the crystals in reference to the X-ray source is at the top. Figure 3(a) presents an overview showing that most crystals grew to a similar thickness during crystallization. Figure 3(b) presents this layer in greater detail, the total thickness of the sample in this cross section is 107 μm and the bulk of the crystallized volume can be estimated to be covered by a glass layer of 48 μm. The thickest μ-cordierite crystal detected during analysis is highlighted by the black arrow and presented in greater detail in Figure 3(c). The tip of this crystal in the prepared cross section is still covered by a glass layer of at least 30 μm.

In order to protect the stability of the sample, only one full cross section was performed while the remaining sides were only cut across the corners. The resulting dimensions of the final sample are presented in Figure 4, the SEM micrographs in Figure 3 were acquired from side 1. Only one edge of side 3 is thinner than the thickness illustrated in Figure 3 while most of the sample exceeds the average thickness of 107 μm measured for side 1.

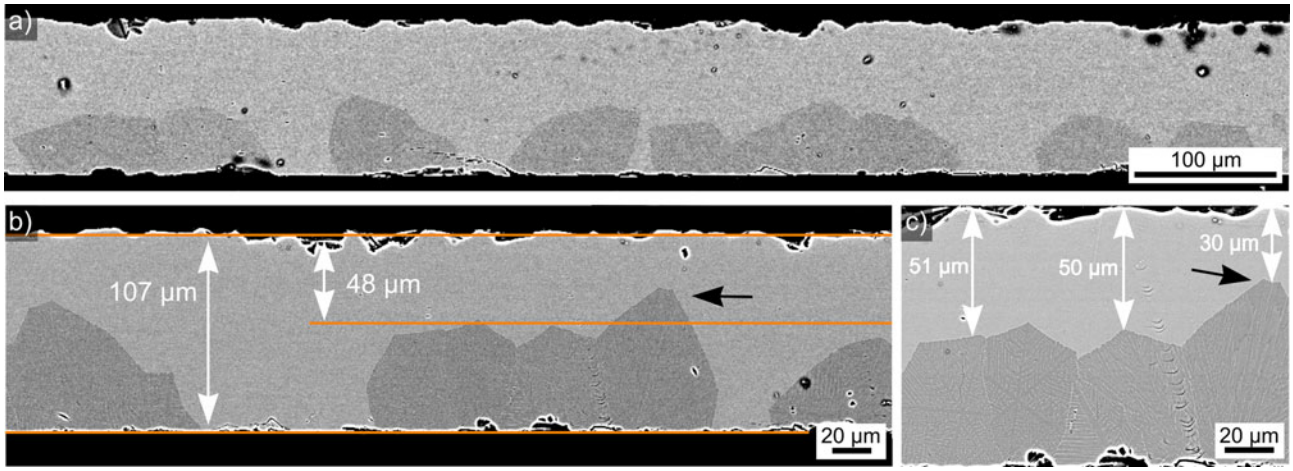

Figure 3. (a) SEM micrograph of a cross section prepared after the final XRD measurement: the μ-cordierite crystals crystallized from the initially polished surface are at the bottom and covered by a layer of glass with respect to the X-ray source. (b) SEM micrograph of the same cross section illustrating that the sample thickness is 107 μm while most of the crystallized volume is covered by a glass layer ca. 48 μm thick. The thickest μ-cordierite crystal located during these measurements is highlighted by the black arrow. (c) SEM micrograph the crystal highlighted in (b) in greater detail (white arrow) to show that even the tip of this crystal is still covered by a glass layer of 30 μm.

https://doi.org/10.1017/S0885715623000052 Published online by Cambridge University Press

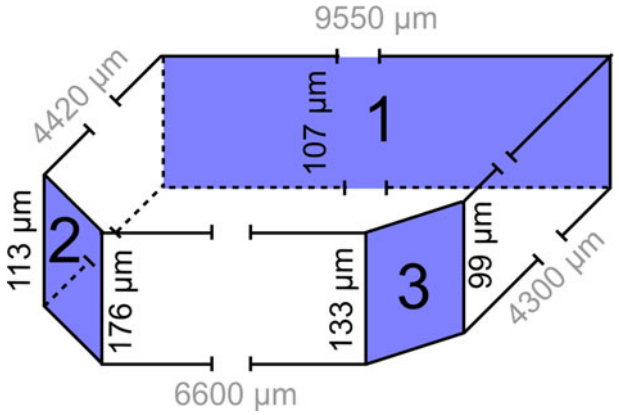

Figure 4. Final sample shape and dimensions after preparing the cross sections at the corners. The thicknesses of the sides 1–3 were measured using SEM micrographs while lengths (gray numbers) were measured using a µm-screw. The XRD patterns (d) and (e) in Figure 2 were acquired from this shape.

The results above show that strong XRD patterns were acquired through an amorphous layer at least 30 µm, but more probably 48 µm, thick at the thinnest side of the sample. Elsewhere the glass layer covering the crystals is even thicker. As the X-rays must penetrate the amorphous layer, interact with the crystals and then again pass through the glass layer to cause a signal at the detector, the significant information depth of XRD must be more than 30 µm and is very likely more than 48 µm.

The simulated, angle-dependent thickness of material contributing 90% or 99% of the detected signal in µ-cordierite, i.e. Eq. (1) discussed below with $I_d/I_0 = 0.9$ or 0.99, are plotted in Figure 5 superimposed onto a background of the crystal layer featuring the thickest µ-cordierite crystal in Figure 3(b). They are approximated to linearity, open circles outline the sin-dependent information depth to illustrate that the approximation is suitable for this application. The respective penetration depths for the diffraction peaks of selected lattice planes are stated above. Considering that the experimental results in Figure 2 do not show any discernible 100 peak but a clear 101 peak of relatively reduced intensity, it would seem the glass layer is thick enough to completely block the 100 signal. Of course this is a low intensity peak, but at $\Theta = 19.6°$ the calculated penetration depths are also at least 7 µm smaller

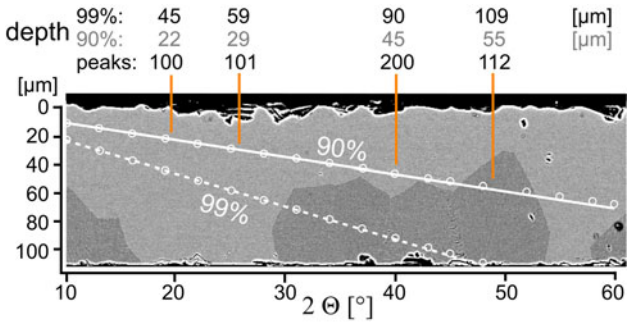

Figure 5. Linearly approximated simulated thicknesses of material contributing 90% or 99% of the detected signal in µ-cordierite for the respective collecting angle Θ plotted over an SEM micrograph of the analyzed crystal layer. Open circles outline the correct sin-dependent depths. The material thicknesses for the diffraction peaks of selected lattice planes are stated.

than at $\Theta = 25.8°$. At $\Theta = 25.8°$, the 90% absorption only just reaches a depth of ~30 µm in the sample, so it is unlikely that the 90% absorption curve is relevant. As the X-rays must penetrate the glass layer twice to produce a signal at the detector, either a tiny fraction of the incoming X-rays (<<1%) are sufficient to produce the detected signal, or the calculations in the used software do not apply to the performed experiment. In any case, the significant information depth of the method should be larger than the depth from which 90% of the reflected X-rays originate.

Alternatively, and e.g. an alternative to simulation software such as PROFEX or the commercial program AbsorbDX, it is possible to correlate these experimental results to Eq. (1) which can be used to calculate the minimal sample thickness necessary for an XRD measurement unaffected by the systematic intensity loss caused by sample penetration: a sample should be as thick as the maximum information depth of the measurement.

$$\frac{I_d}{I_0} = e^{-\mu \cdot \rho \cdot d} \text{ (Lambert-Beer Law)} \quad (1)$$

where I_d is the exit beam intensity, I_0 is the entry beam intensity, μ is the mass absorption coefficient (cm^2/g), ρ is the density of the material (g/cm^3), and d is the sample thickness (cm). The mass absorption coefficient of a material may be calculated using Eq. (2) and the μ-values of the elements e.g. stated in Table 1 of Henke et al. (1982).

$$\mu = \sum x_i * \mu_i \quad (2)$$

where x_i is the mass fraction of the element and μ_i is the mass absorption coefficient of the element (cm^2/g). Applying various values for I_d/I_0 showed that a cut-off value of 77.5% leads to the thickness of ca. 30 µm while a cut-off value of 67% leads to the thickness of ca. 48 µm. As the final polishing step removed a rather large amount of material (ca. 70 µm) and the XRD patterns (d) and (e) in Figure 2 are quite strong, it seems plausible to assume that the true significant information depth of XRD in the chosen µ-cordierite glass layer system is larger than 48 µm but smaller than 118 µm. This is in agreement with the value proposed for SiO_2 (Wisniewski et al., 2013). A thickness of ca. 118 µm is reached with $I_d/I_0 = 37\%$ in the chosen glass.

Applying these cut-off values to Eq. (1) using the values of other materials leads to the values in Table I. It presents calculated upper and lower limits of the significant information depth of XRD in phases discussed here as well as some selected for their density. As expected, the absolute difference between the depths becomes less important as they decrease. Note that it is larger for Ag than for Nd despite the higher density of Ag because Nd has a much larger mass absorption coefficient. Performing the calculation for Sr-fresnoite using Co Kα radiation leads to $\mu = 125.6776$ cm^2/g and an information depth larger than 9.4 µm but smaller than 30.8 µm. Hence, the 10 µm stated by Renoirt et al. (2019) are a bit low.

The significant information depth outlined above explains why multiple crystallographic textures resulting from a continuous growth selection (Wisniewski et al., 2012a, 2012b; Renoirt et al., 2019) can be indicated within the same XRD pattern. It should be remembered that the amorphous layer dampening the XRD signal in the performed experiment

https://doi.org/10.1017/S0885715623000052 Published online by Cambridge University Press

TABLE I. Calculated boundaries for the significant information depth (ID) in materials discussed above and some elements selected for their density using Cu Kα radiation.

Material	Density (g/cm^3)	Calculated μ (cm^2/g)	ID larger than (µm)	ID smaller than (µm)
Low cristobalite (SiO_2)	2.33	35.0988	48.9	121.5
µ Corierite ($MgAl_2Si_3O_{10}$)	2.59	32.0071	48.3	119.9
Sr-Fresnoite ($Sr_2TiSi_2O_8$)	3.88	83.0979	12.4	30.8
Neodym (Nd)	7.01	411.0000	1.4	3.5
Silver (Ag)	10.05	207.0000	1.8	4.6
Platinum (Pt)	21.45	204.0000	0.9	2.3

It is approximately **larger than** the value resulting from $I_d/I_0 = 67\%$ but **smaller than** that resulting from $I_d/I_0 = 37\%$.

only provides background noise to the signal. In a sample containing multiple polycrystalline layers, the strong signal from the topmost layers will dominate the weaker signal from layers further in the bulk and possibly reduce this depth.

While the presented experiment can clearly be improved by a more precise sample preparation and e.g. producing a crystal layer of more homogeneous thickness, the results sufficiently prove that the significant information depth of XRD is frequently underestimated. This depth is relevant to all XRD measurements performed on compact/bulk samples, especially solar cell materials, thin films, surface-crystallized glass-ceramics, layered composites, and all samples showing a texture evolution perpendicular to the analyzed surface.

IV. CONCLUSION

The significant information depth of XRD is larger than often assumed, especially in low absorption materials. For the analyzed sample of the composition $Mg_2Al_4Si_5O_{18}$ with a density of ~ 2.6 g/cm^3, it is most likely more than 48 µm but less than 118 µm when using Cu Kα radiation in the applied equipment. Assuming this depth is comparable among different machines, it should hence be larger than the depth from which 90% of the reflected X-rays originate. Alternatively, this thickness can be calculated by implementing a value of $I_d/I_0 = 67\%$ to the calculation for the minimal sample thickness necessary for perform an XRD measurement unaffected by the systematic intensity loss caused by sample penetration.

ACKNOWLEDGMENTS

Results incorporated in this paper have received funding from the European Union's Horizon 2020 research and innovation program under the Marie Skłodowska-Curie grant agreement No. 665790.

CONFLICT OF INTEREST

There are no conflicts of interest to declare.

REFERENCES

Allmann, R. 2003. *Röntgenpulverdiffratometrie*. New York, Springer.

Birkholz, M. 2006. *Thin Film Analysis by X-Ray Scattering*. Weinheim, Wiley-VCH.

Diaz-Mora, N., E. D. Zanotto, R. Hergt, and R. Müller. 2000. "Surface Crystallization and Texture in Cordierite Glasses." *Journal of Non-Crystalline Solids* 273: 81–93.

Fokin, V. M., E. D. Zanotto, N. S. Yuritsyn, and J. W. P. Schmelzer. 2006. "Homogeneous Crystal Nucleation in Silicate Glasses: A 40 Years Perspective." *Journal of Non-Crystalline Solids* 352: 2681–714.

Hartenbach, I., S. F. Meier, and T. Schleid. 2006. "ζ-$Y_2[Si_2O_7]$: Ein neuer Strukturtyp in der Yttrialit-Reihe." *Zeitschrift für Naturforschung* 61B: 1054–60.

Henke, B. L., P. Lee, T. J. Tanaka, R. L. Shimabukuro, and B. K. Fujikawa. 1982. "Low-Energy X-Ray Interaction Coefficients: Photoabsorption, Scattering, and Reflection." *Atomic Data and Nuclear Data* 27: 1–144.

Holder, C. F., and R. E. Schaak. 2019. "Tutorial on Powder X-Ray Diffraction for Characterizing Nanoscale Materials." *ACS Nano* 13: 7359–65.

Keshavarzi, A., W. Wisniewski, and C. Rüssel. 2013. "Surface Crystallisation of Yttrium Aluminum Garnet from a Silicate Glass." *CrystEngComm* 15: 5425–33.

Liu, J., R. S. Saw, and Y.-H. Kiang. 2010. "Calculation of Effective Penetration Depth in X-Ray Diffraction for Pharmaceutical Solids." *Journal of Pharmaceutical Sciences* 99: 3807–14.

Mendenhall, M. H., A. Henins, L. T. Hudson, C. I. Szabo, D. Windover, and J. P. Cline. 2017. "High-Precision Measurement of the X-Ray Cu Kα Spectrum." *Journal of Physics B: Atomic, Molecular and Optical Physics* 50: 115004.

Müller, R., E. D. Zanotto, and V. M. Fokin. 2000. "Surface Crystallization of Silicate Glasses: Nucleation Sites and Kinetics." *Journal of Non-Crystalline Solids* 274: 208–31.

Pannhorst, W. 2000. *Surface Nucleation*. Charleroi, International Commission on Glass.

Renoirt, M.-S., N. Maury, F. Dupla, and M. Gonon. 2019. "Structure and Properties of Piezoelectric Strontium Fresnoite Glass-Ceramics Belonging to the Sr–Ti–Si–Al–K–O System." *Ceramics* 2: 86–97.

Spieß, L., G. Teichert, R. Schwarzer, H. Behnken, and C. Genzel (Eds.). 2009. *Moderne Röntgenbeugung 2. Ed*. New York, Springer.

Wisniewski, W., and C. Rüssel. 2021. "Oriented Surface Nucleation in Inorganic Glasses – A Review." *Progress in Materials Sciences* 118: 188758.

Wisniewski, W., M. Nagel, G. Völksch, and C. Rüssel. 2010a. "Electron Backscatter Diffraction of Fresnoite Crystals Grown fom a Surface of a $2BaO{\cdot}TiO_2{\cdot}2.75SiO_2$ Glass." *Crystal Growth & Design* 10: 1414–8.

Wisniewski, W., T. Zscheckel, G. Völksch, and C. Rüssel. 2010b. "Electron Backscatter Diffraction of $BaAl_2B_2O_7$ Crystals Grown from the Surface of a $BaO{\cdot}Al_2O_3{\cdot}B_2O_3$ Glass." *CrystEngComm* 12: 3105–11.

Wisniewski, W., C. A. Baptista, M. Müller, G. Völksch, and C. Rüssel. 2011. "Surface Crystallization of Cordierite from Glass Studied by High-Temperature X-Ray Diffraction and Electron Backscatter Diffraction (EBSD)." *Crystal Growth & Design* 11: 4660–6.

Wisniewski, W., M. Patschger, and C. Rüssel. 2012a. "Sr-Fresnoite Surface Crystallisation in a $2SrO{\cdot}TiO_2{\cdot}2.75\ SiO_2$ Glass Studied by EBSD." *CrystEngComm* 14: 5425–33.

Wisniewski, W., M. Patschger, and C. Rüssel. 2012b. "Piezoelectric Glass-Ceramics Produced via Oriented Growth of $Sr_2TiSi_2O_8$ Fresnoite: Thermal Annealing of Surface Modified Guenched Glasses." *CrystEngComm* 14: 7368–73.

Wisniewski, W., S. Berndt, M. Müller, and C. Rüssel. 2013. "Stress Induced Texture Formation in Surface Crystallized SiO_2 Glass." *CrystEngComm* 15: 2392–400.

Wisniewski, W., K. Thieme, and C. Rüssel. 2018a. "Fresnoite Glass-Ceramics – A Review." *Progress in Materials Science* 98: 68–107.

Wisniewski, W., A. J. Fernández-Carrión, P. Schöppe, C. Rüssel, and M. Allix. 2018b. "Oriented Nucleation and Crystal Growth in SrO–Al_2O_3–SiO_2 Tectosilicate Glasses." *CrystEngComm* 20: 3455–66.